



# Geophysical and borehole investigations of subsurface hazardous karsts in Ar-Riyadh city, Kingdom of Saudi Arabia

Ahmed K. Abd El-Aal<sup>1,2</sup> · Mohamed K. Salah<sup>3,4</sup> · Mohammad Khalid Ansari<sup>5</sup> · Mashud Ahmad<sup>5</sup> · Trilok Nath Singh<sup>5</sup>

Accepted: 12 June 2021 / Published online: 20 June 2021

© The Author(s), under exclusive licence to Springer-Verlag GmbH Germany, part of Springer Nature 2021

## Abstract

Geophysical and borehole investigations were carried out to explore the sites of subsurface buried cavities and related subsidence in Ar-Riyadh city, Kingdom of Saudi Arabia (KSA). Traditional ground probing practices were not adequately conducted in the city due to various reasons including lack of technology at a time, economic factors, the ambient general culture, and time constraints. Consequently, locations of near-surface buried hazardous cavities for proposed development projects in the studied area are essentially unknown. The geophysical studies are represented by the interpretation of ground penetrating radar (GPR) images, while the borehole investigations were done through five drilled boreholes (BHs). A good match between the results of the two methods has been found indicating the usefulness of radar techniques to identify the ground conditions prior to major engineering projects in karstic regions such as Ar-Riyadh. In addition to locating major cavities in a city underlain by limestone bedrock, crucial recommendations have been proposed to be implemented before and/or during the design and construction of major foundations in the area.

**Keywords** Karstic hazards · Ground-penetrating radar (GPR) · Geophysical exploration · Borehole investigations (BHI) · Ar-Riyadh city

## Introduction

The Kingdom of Saudi Arabia (KSA) is well known for its hyper-arid climatic conditions and the widespread occurrence of carbonates and evaporite beds which cover approximately 60% of its total surface area (Youssef et al. 2016). These rock types are highly susceptible to dissolution and karstification, hence posing serious threats for construction

activities and could cause major socio-economic losses. Karsts develop when soluble materials (mainly evaporites and carbonates) exist underground; which dissolve later removing a volume of the rock framework followed subsequently by collapse or subsidence. Recently, Festa et al. 2012; Abdeltawab 2013, Youssef et al. 2011, 2012, 2016, Abd El Aal 2017, Abd El Aal and Masoud 2017; and Abd El Aal et al. 2020, documented the existence of many sinkholes and karst features in different geologic environments. Karstic processes have adverse effects on infrastructures and buildings and can cause significant property damages (Pueyo Anchuela et al. 2015). These features pose huge challenges for construction activities such as ground subsidence and/or infrastructure collapse (Cueto et al. 2019). Subsidence is induced by the dissolution of evaporites and carbonates underlying the surficial alluvium (Pueyo Anchuela et al. 2014).

A variety of methods have been employed in the KSA to identify the karst-related features including sinkholes and cavities. Field reconnaissance surveys, topographical mapping, routine geological studies, and remote sensing techniques, along with interviewing local people are some of the methods used to identify and locate cavities in the

✉ Mohamed K. Salah  
ms264@aub.edu.lb

Ahmed K. Abd El-Aal  
Ahmed\_aka80@yahoo.com; Akahmed@nu.edu.sa

<sup>1</sup> Geology Department, Faculty of Science, Al-Azhar University, Assuit Branch, Egypt

<sup>2</sup> Civil Engineering Department, Faculty of Engineering, Najran University, 1988, Najran, Saudi Arabia

<sup>3</sup> Department of Geology, American University of Beirut, Riad El Solh, Beirut 1107 2020, Lebanon

<sup>4</sup> Geology Department, Faculty of Science, Tanta University, Tanta 31527, Egypt

<sup>5</sup> Department of Earth Sciences, Indian Institute of Technology Bombay, Mumbai, Maharashtra, India

kingdom. Meanwhile, the geological and geomorphological field investigations are also useful for the location and characterization of these hazardous features.

Ground-Penetrating Radar (GPR) is a very useful geophysical tool for near-surface studies such as shallow groundwater exploration, archeology, and surficial karsts, dolines, and sinkholes (e.g., Pueyo et al. 2009, 2013). It is the most suitable method to explore shallow subsurface faulting, underground cavities; either natural or man-made, and groundwater contamination. If other geotechnical methods such as borehole investigations, outcrops in quarries, trenches, and surface data are used in conjunction with the GPR, they together are more powerful for the identification of the cavities and the overall shallow subsurface setting (Al-Sayari and Zötl 1978; Smith 1986; Elawadi et al. 2001; El-Qady et al. 2005; Mochales et al. 2008; Pueyo Anchueta et al. 2014). Radar facies refer to groups of radar reflections with characteristic continuity, configuration, amplitude, interval velocity, attenuation, and dispersion that differ from those of neighboring groups. These facies are useful in delineating shallow subsurface anomalies related to lithology, fracturing, fluid content, and salinity (Forte et al. 2012; Pueyo Anchueta et al. 2014). Compared to other geophysical techniques, the GPR is a quick survey method, very sensitive to the shallow subsurface, provides high-resolution images, and permits the isolation of many forms of urban noise that would preclude the use of other geophysical methods.

The GPR is an electromagnetic geophysical exploration technique that responds to changes in the electromagnetic properties of shallow subsurface materials; mainly their electrical conductivity and electrical permittivity (Daniels 2005, 2014). Recently, it has become a common geophysical tool used to detect voids, buried sinkholes, fractures, karst features, and solution-filled cavities mainly within evaporites and carbonate sequences. It uses high-frequency electromagnetic waves that penetrate the shallow subsurface and is reflected back from certain boundaries across which there are changes in the dielectric constant, hence providing information on the subsurface (Davis and Annan 1989; Annan and Davis 1992). The transmitted waves undergo multiple reflections and hence are damped during propagation. These analog signals are converted to a digital form and are displayed as images known as radargrams in the processing stage. Radar profiles are time-distance plots where the horizontal distance along a profile and the two-way travel time are drawn along the axes with the amplitudes of the reflected waves being displayed against the corresponding travel times. In general, the principles of the GPR method are similar to those of the seismic reflection method; however, the GPR, reflections come from obstacles and/or strata having different electrical impedance underneath the ground which changes the propagation velocity of the radar signals. Seismic reflections, on the other hand, are produced at

discontinuities separating layers of different acoustic impedance. Contrasts in the electrical impedance of the shallow subsurface may result from, for instance, the soil type, grain size distribution, the void ratio, moisture content, and salinity (Knight and Nur 1987; Davis and Annan 1989; Annan et al. 1991; Olhoeft 1994; Annan 2001). Thus, in the context of the GPR technique, an interface is defined as the boundary between materials of different electromagnetic impedance. The GPR investigation capability is influenced by two parameters; first is the antenna's central frequency, antenna's characteristics, as well as the power of the input device; and second, by the characteristics of shallow materials to be investigated (ground/strata). If the antenna's frequency is high it will provide high resolution but shallow penetration depth; conversely, a low-frequency antenna provides higher penetration depths but with a reduced resolution (Daniels 2014). Characteristics of subsurface materials such as a low-resistivity soil and/or high clay content can simply disperse the waves in the subsurface and thus influence the quality of GPR images. So, strong radar reflections come from air-filled voids and/or layers of water-saturated sediments. The early 1980s witnessed most of the improvements and the spread of the commercial applications of the GPR technique that were documented in the literature. In its early usage, the system was exclusively using the impulsive time-domain, and the applications of GPR were limited to the identification of voids, measuring the thickness of ice and coal layers, and detection of utilities such as cables and tubes. At present, the applications have been extended to other different fields and represent now an essential component of a standard geophysical exploration program.

In this study, we present the use of GPR/borehole investigations for locating buried cavities and the near-surface soil and bedrock conditions in Ar-Riyadh city, KSA. We emphasize the importance of the combined use of both techniques in the appraisal of the shallow subsurface conditions of the soil/bedrock which are crucial before proposed major constructions in new communities. The data acquired from the drilled boreholes are used to find out the volume of the karst-affected area and to figure out conceivable mitigation measures. In addition, recommendations have been formulated as well as solutions for possible post-construction problems.

## Structural and geological setting

The studied region is situated at the center of Ar-Riyadh city (Fig. 1). Structurally, Ar-Riyadh area is, in general, a part of a large sub-horizontal, northeasterly-dipping homocline (Hughes and Lindsay 2017). This homocline shows a minor flexure to the south of Ar-Riyadh area. This structural disturbance is thought to be related to the great central Arabian Platform. Towards the south, the homocline is also disrupted

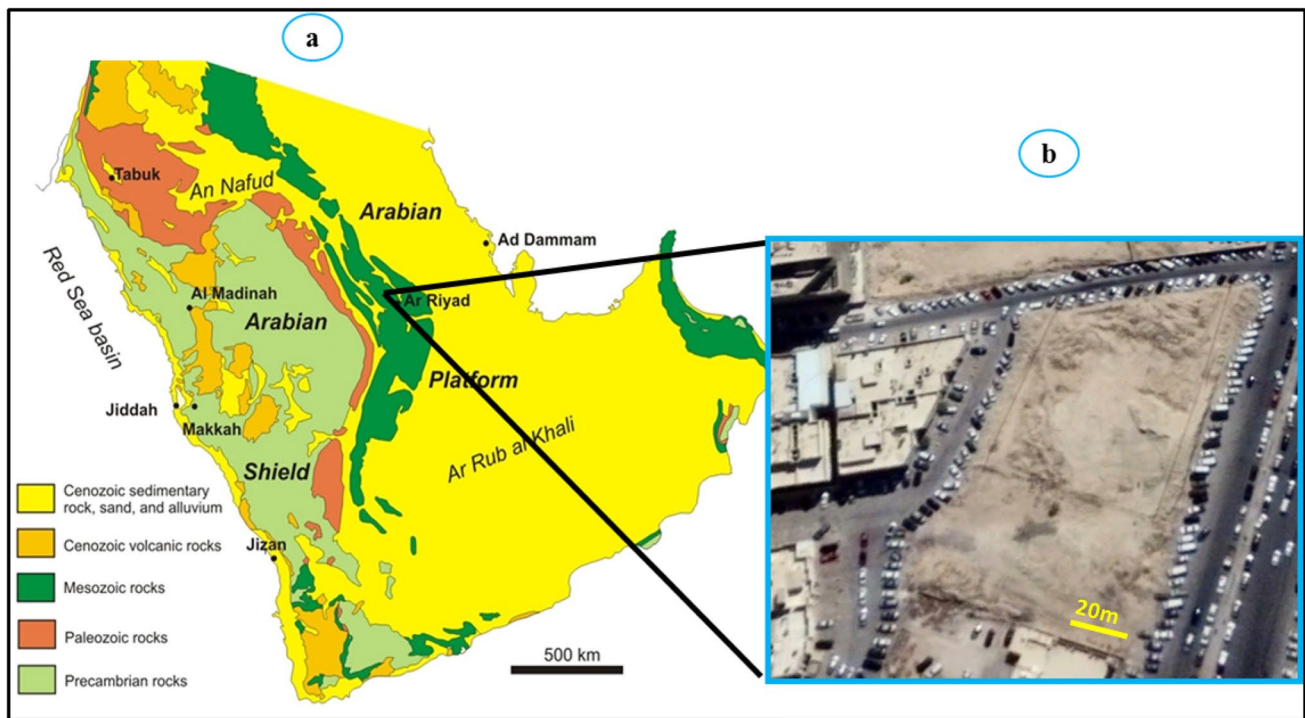


**Fig. 1** Location map of study area in the eastern margin of the Arabian shield (a), and the center of Ar-Riyadh city, KSA (b)

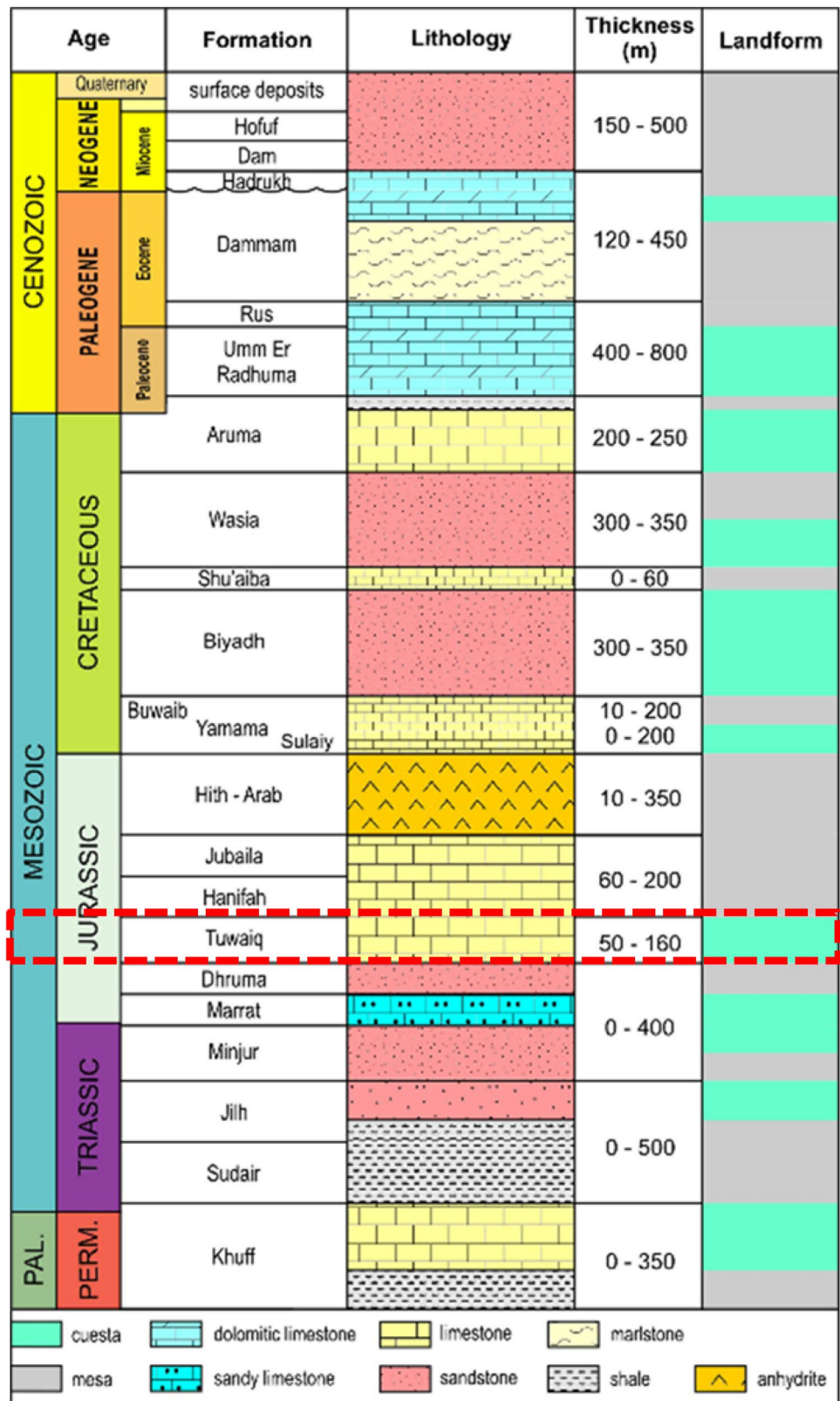
by a series of west- to east-trending grabens in addition to the extensive collapse structures that created the evaporitic formations of the late Mesozoic (Hughes and Najj 2008). Another major structural disturbance was created by the collapse affecting the Arab Formation, in general, and the Hith Anhydrite member in particular (Sharief et al. 1991). The anhydrites were altered into gypsum and only solution residues remain today. These residues were produced by the dissolution of about 130 m of an evaporite succession; leading to extensive brecciation of the limestone rocks. To the north and northeast of Ar-Riyadh, Al Butayn and Wadi Al Silay depressions were formed mainly by collapses. Fracturing and brecciation, formed as direct consequences of the collapses, created preferential routes for the rainwater that further enhanced extensive weathering and dissolution of the limestone rocks.

Sheet gravels of the inactive type which commonly occurs as Cuesta piedmonts and alluvial fans merging in the plains at the valley mouths are present in the area. Moreover, the inactive sheet gravels are also found at the edges of the graben structures and in the deeply incised wadis of the Tuwaiq plateau, and in large depressions such as Al Butayn and Dilam. The present active wadi alluvium is similar to the one in the nearby Wadi Butayn and consists of subrounded gravel and pebbles of Mesozoic limestones (Vaslet et al. 1991).

According to Amin and Bankher (1997), the main karst rock units in the Arabian Platform are the Mesozoic-aged Arab, Hith, Sulaiy, and the Aruma (Badanah, and Zal-lum) formations, as well as the Cenozoic Umm Er Radhum (Edgell 1990), Rus, Dammam, Dam, and Sirhan formations. These formations are characterized by a general easterly-dipping trend and a homoclinal structure that tends to form actuate belts of younger sediments towards the east. Within the study area, the Tuwaiq Escarpment is the most outstanding cuesta, formed in the subsurface bedrocks. It is mainly composed of Jurassic white to yellow, massive, karstic limestones (Fig. 2). In Riyadh area, the cliff is about 200 m high, and the Jurassic Arab and Hith formations (Fig. 2), which are composed of considerable evaporitic rocks are also exposed. These two formations are rarely exposed on the surface because they have undergone severe attrition mainly by dissolution. Subsurface dissolution of these formations and the subsidence of the overlying sediments have generated numerous huge subsidence dolines, karsts, and sinkholes (Vaslet et al. 1991).

The Early Cretaceous Yamama Formation is made up of alternating calcareous facies consisting of calcarenite, calcarenitic limestone, and fine-grained limestone. In particular, the exposed rocks of the Yamama Formation show alternating white to grayish, yellowish bioturbated clayey limestone and brownish bioclastic to pelletoidal calcarenite, with local enrichment in clasts and bivalves. An

**Fig. 2** General stratigraphic succession of the Mesozoic in Saudi Arabia including the main carbonate and evaporite karstic units with thicknesses measured at the type locality (modified from Powers et al. 1966). The dashed red rectangle denotes the studied Jurassic Tuwaiq Formation



average thickness of about 40 m was recorded in An-Nasim district (study area), to the northwest of Ar-Riyadh. Clean leached calcarenite and calcirudite are the main rock types

exposed at the type locality to the south of Ar-Riyadh. Elsewhere, mud-rich sediments, calcarenite limestone, and very thin layers of shale are occasionally encountered

(Powers et al. 1966). It is also important to mention that the upper part of the Yamama Formation is very bioturbated and is also intersected by several hardgrounds that probably indicate breaks in sedimentation. Bioclastic and lithoclastic calcarenite channels are also found towards the top of this formation.

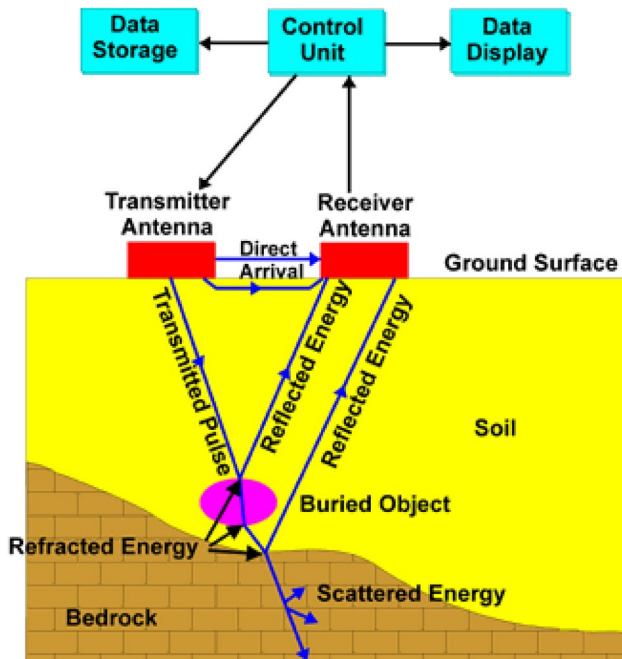


**Fig. 3** A typical GPR system with a transmitter and an antenna (Takahashi 2006)

## Data and methods

### Ground-penetrating radar (GPR)

The collected GPR data was acquired using SIR 3000 shielded antenna with a central frequency of 100 MHz. The locations of the profiles were determined initially by the GPS. The spacing between two adjacent profiles varies between 1–1.5 m at maximum. The data acquisition was carried out along 24 grids distributed along parallel and orthogonal lines. A typical system, with both transmission and reception antennae coupled together in which the transmitter antenna generates a pulse of electromagnetic radiation in all possible directions, is used (Fig. 3). A metallic shield usually encases this joint system to restrict those signals traveling along directions not aligned with the vertical (Audru et al. 2001). Field surveying was conducted by a team of researchers and assistants (Fig. 4a–d). The antenna throws a bunch of electromagnetic waves in a conical form which hit the target reflector then reflected back. GPR data acquisition system is designed so that it does not show individual amplitude traces from the subsurface. Rather, it stacks several such traces in the horizontal direction to provide a line scan. All the line scans during particular profiling (Fig. 5a–c) are stacked together to form a complete GPR profile (Neal 2004). The GPR data were collected along twenty-four longitudinal and traverse grids comprising a total of 365 readings. The large number of profiles (Fig. 6) helps to accurately detect subsurface anomalies. The surveyed grids, number of profiles in



**Fig. 4** Field GPR data acquisition a–d in one of the investigated sites

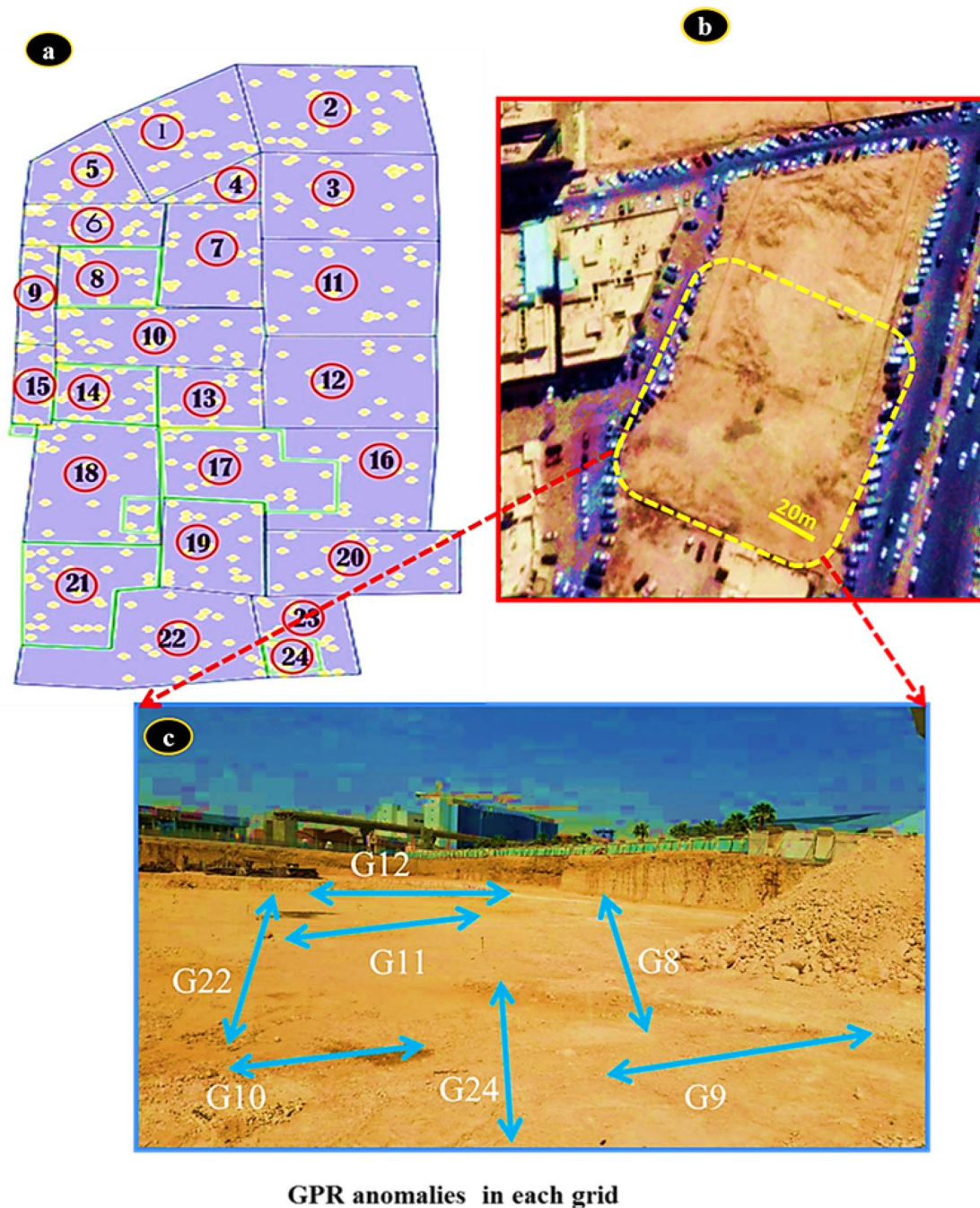


**Fig. 5** a Locations and numbers of grids set up for the GPR surveying; b and c some GPR profiles along nearly N-S and E-W directions

each grid, their respective lengths and directions are shown in Table 1.

Some acquisition parameters were adjusted during fieldwork to avoid delay in subsequent processing. These include initial high-pass filtering, application of time gain function, infinite impulse response (IIR) filter, and sometimes finite impulse response (FIR) filters. Any antenna with a particular frequency denomination used for the GPR survey generates electromagnetic waves in a range

of frequencies modeled as a Gaussian distribution centered on that frequency (Daniels 1996). An IIR filter is a recursive filter where the current output depends on previous outputs, whereas the FIR filter is a linear combination of a finite number of samples of the input signal. The FIR filters do not use the feedback system and are commonly used to attenuate the short-term fluctuations in the amplitudes in relation to long term trends (Oppenheim et al. 2003).

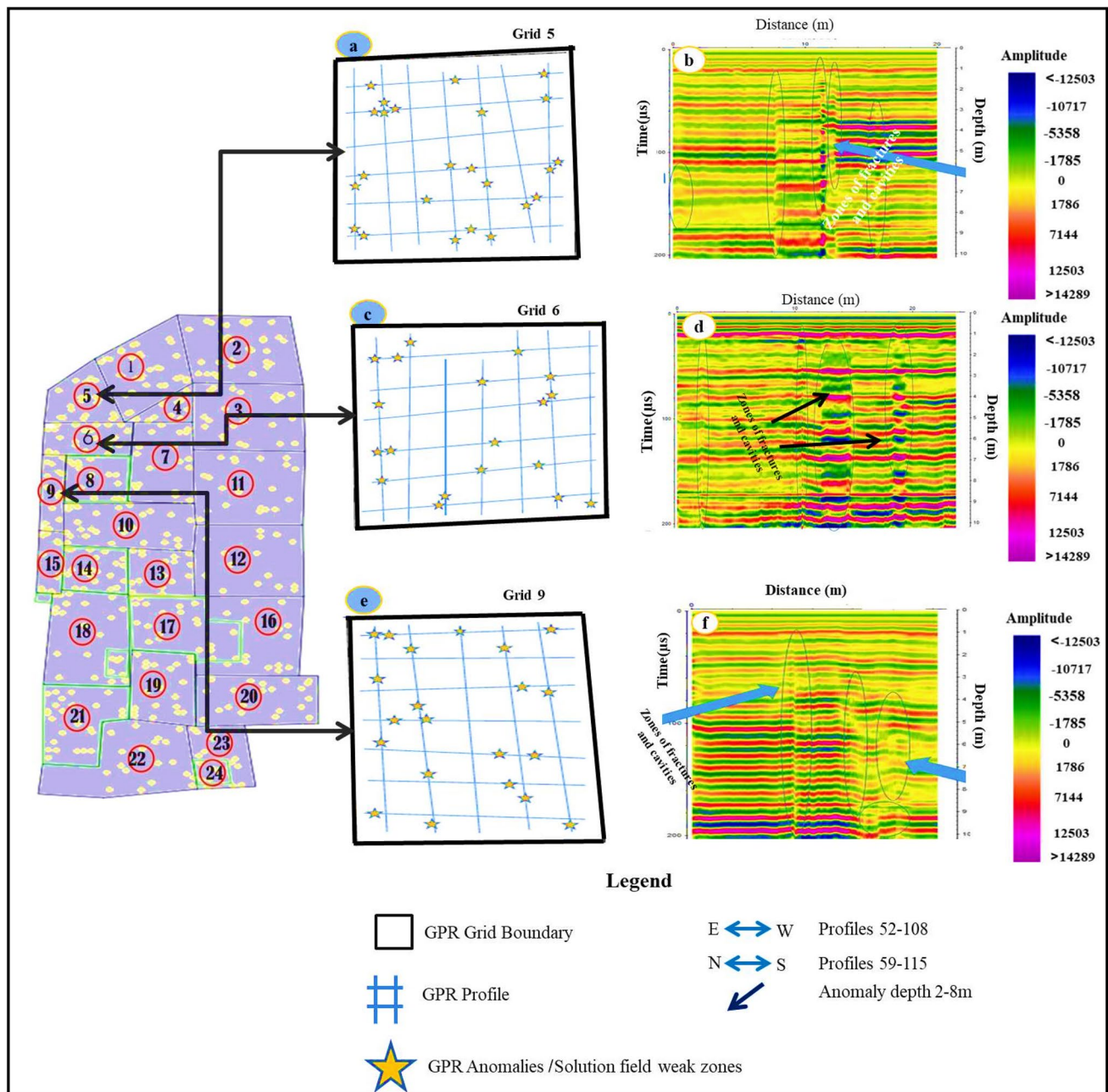


**Fig. 6** Example of GPR profiles a–f for the same transect for 100 MHz, indicating that some changes in resolution of GPR profiles can be detected, and a similar penetration depth can be illustrated at both profiles

After initial on-field processing of the data, some post-acquisition processing is required for feature detection and interpretation (Fisher et al. 1996). Post-processing was performed with RADAN program (Geophysical Survey System Inc. 2005, 2008) and comprises the following steps: (a) editing of header file; (b) normalization of the horizontal scale; (c) bandpass frequency filtering to get rid of high and low frequencies; (d) application of automatic gain control (to compensate for the decrease in amplitude because of the geometrical spreading), and (e) migration:

moving reflection events generated at dipping reflectors to their actual positions.

The anomalous areas can be identified by analyzing a combination of some main variables in the GPR data. These include (1) the reflectivity contrast indicates changes in layer lithology; (2) the amplitude and phase of the signals generated from an anomalous area indicate loose materials and/or cavities; (3) underground highly-conductive materials (e.g., facilities) render the identification of anomalous features very difficult or nearly

**Table 1** Grid numbers, number of profiles, their orientation and depth ranges sampled by the GPR method as well as the description of the subsurface cavities and karstsAs well as the description of the subsurface cavities and karsts

Grid no.	No of profiles	E-W profiles	N-S profiles	Depth (m)	Description
G1	1–12	1–6	7–12	1.5–8	Solution-filled fractures, cavities, and weak zones are detected at most grids
G2	13–26	13–19	20–26	1.5–8	
G3	27–37	27–32	33–37	1.5–8	
G4	38–51	38–42	43–51	1.5–8	
G5	52–64	52–58	59–64	1.5–8	
G6	65–77	65–71	72–77	1.5–8	
G7	78–89	78–83	84–89	1.5–8	
G8	90–103	90–96	97–103	1.5–8	
G9	104–115	104–108	109–115	1.5–8	
G10	116–128	116–123	124–128	1.5–8	
G11	129–144	129–138	139–144	1.5–8	
G12	145–165	145–156	157–165	1.5–8	
G13	166–178	166–172	173–178	1.5–8	
G14	179–189	179–180	181–189	1.5–8	
G15	190–209	190–196	197–209	1.5–8	
G16	210–225	210–218	219–225	1.5–8	
G17	226–256	226–230	231–256	1.5–8	
G18	257–287	257–265	266–287	1.5–8	
G19	288–310	288–300	301–310	1.5–8	
G20	311–320	311–315	316–320	1.5–8	
G21	321–330	321–325	326–330	1.5–8	
G22	331–339	331–335	336–339	1.5–8	
G23	340–350	340–345	346–350	1.5–8	
G24	351–365	351–357	358–365	1.5–8	

impossible; (4) zones of low reflectivity within a section may indicate a solution cavity; and zones of high reflectivity, on the other hand, indicate an increase in fracturing within the parent rock; limestone in this case; (5) a sudden increase in reflectivity extending vertically downward is indicative of changes in lithology; generally an effect of cementation and recrystallization; and (6) the travel time of radio pulses through the material gives an indication of the layer thickness or depth to embedded features (cracks or fractures) such as those detected in the present study.

Although the interpretation of GPR data is a very objective-dependent activity, it is also very subjective as it depends also on the individual doing the interpretation. Moreover, the radar wavelength plays a vital role in the identification of the resolvable thickness of a geological layer or offset of a horizon. Cavities can be identified in radar sections because they generate different reflection patterns or terminations and/or apparent near-vertical offsets of laterally continuous reflections which are distinctly different from the continuous reflections generated by sub-horizontal and trough-like boundaries of several sedimentary units (Fig. 6a–f) (Gross et al. 2002).

## Borehole analysis and investigations

A total of five boreholes were drilled in the study area for geotechnical investigations and to validate the geological model obtained from the interpreted GPR data. The boreholes were drilled at selected sites down to a maximum depth of 10 m below the ground surface (Fig. 7a, b). Locations of the boreholes have been selected to verify the observed GPR anomalies and to accurately locate the karst features. The five BHs were drilled to a maximum depth of 10 m and terminated when the limestone bedrock was encountered. Drilling started at the foundation level which is located over a fractured limestone characterized by a very low strength and solution cavities (Fig. 7). The borehole investigations are represented by the RQD, TCR, and field permeability tests which are briefly summarized in the following paragraphs.

The Rock Quality Designation (RQD) is a rough estimate of the jointing or fracturing strength of a rock, taken as a percentage of the drill core at lengths of more than 10 cm. The high-quality rocks have RQD of more than 75%, while low quality rocks have RQD of less than 50% (Trivedi 2015).

**Fig. 7** **a** General view of the site under investigation, **b** A drilling machine, **c** Retrieved cores showing the highly fractured limestone rock, and **d** A close-up view of one core sample with some solution cavities

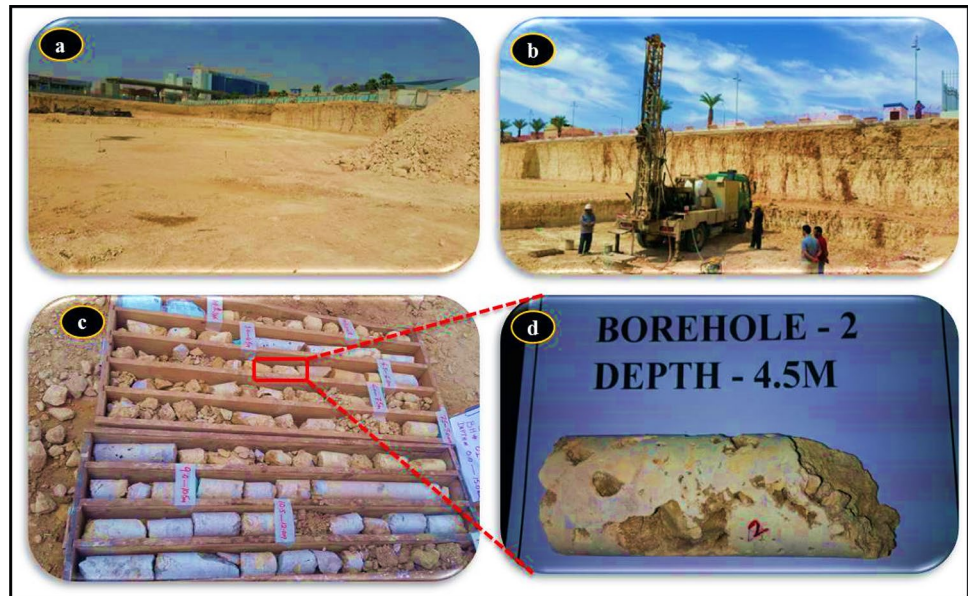


**Table 2** Classification of RQD according to Deere (1964) which is used in the present work

Class	RQD	Description
I	100–90	Excellent
II	90–75	Good
III	75–50	Fair
IV	50–25	poor
V	< 25	Very poor

There are several interpretations for the RQD values; with the most widely used are those developed by Deere (1964). The RQD values obtained from the boreholes are given in Table 2.

The total core recovery (TCR) is defined as the ratio between the recovered core and the total drilled run time (Nicholls 2012). The length reported as the actual depth penetrated by the driller is the core run. The TCR contains both the strong core as well as the non-solid (or non-intact) core. The recovery is then calculated using a tape measure and are recorded as lengths (not determined as ratios), and this length is incorporated into the log program for the borehole (Valentine and Norbury 2011). The TCR test was done on selected cores, and is calculated simply as:

$$\text{TCR (\%)} = \left( \frac{L_{\text{sum of core pieces}}}{L_{\text{tot core run}}} \right) \times 100 \quad (1)$$

where TCR is the total core recovery,  $L_{\text{sum of core pieces}}$  is the summation of length of core pieces, and  $L_{\text{tot core sum}}$  is the total length of core run.

The falling head permeability test was carried out to assess the permeability of the fractured limestone bedrock in the study area (Eid 2007). Tests were done following the procedure given in BS 5930 (2015). The site geologist

**Table 3** Results of the in-situ permeability test for borehole 5 (BH5)

Time (sec)	Water drop (cm)	H	(H/H <sub>0</sub> )
0	0.0	450.00	1.00
60	100.0	350.00	0.78
120	128.0	322.00	0.72
180	135.0	315.00	0.70
300	140.0	310.00	0.69
600	145.0	305.00	0.68
900	150.0	300.00	0.67
1800	182.0	268.00	0.60
2700	197.0	253.00	0.56
3600	216.0	234.00	0.52
5400	244.0	190.00	0.42
7200	260.0	180.00	0.40
9600	274.0	160.00	0.36
10,800	274.0	143.00	0.32

monitoring the drilling of the well records additionally the depth of water loss and its quantity to locate the karsts and solution cavities in the calcareous bedrock foundation. The falling head data of the *in-situ* permeability test conducted at borehole 5 are given in Table 3, and presented in Fig. 8. An open hole was left at the base of the borehole to allow for water seepage into the fractured rocks. As described in Eid (2007), the permeability coefficient (K) was calculated from the following equation:

$$K = \frac{A}{FT} \quad (2)$$

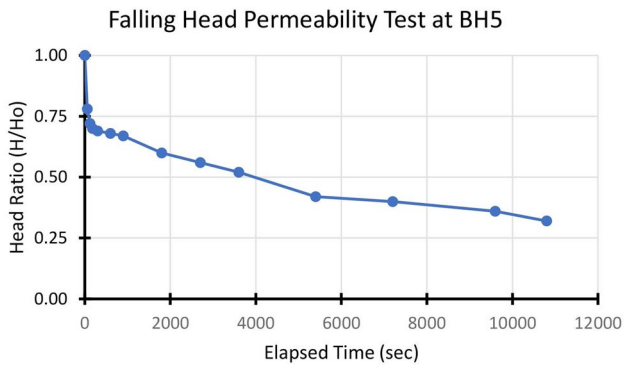


**Fig. 8** The field permeability test conducted for borehole 5

where  $A$  is the borehole area ( $\text{cm}^2$ ),  $F$  is the intake factor (in  $\text{cm}$ ) which is a function of the borehole diameter and the vertical length of the open hole below the casing, and  $T$  is the time lag (sec). The estimated permeability coefficient at borehole 5 is  $1.93 \text{ cm/sec}$  which is relatively large.

### Results and discussion

The investigated area has a top layer composed of a mixture of silt, sand, and gravels overlying a layer of weathered and fractured limestone bedrock. Obtained RQD data are very low varying from 8 to 39 (Fig. 9), indicating fractured and highly weathered limestone rocks (Fig. 7). The lowest RQD

values are detected at the surface but increase downward. Borehole logs indicate that some subsurface cavities are found at a depth of 3.0–3.50 m in borehole 2; at a depth of 4.0 m in BH3, and at a depth of 2.5–3.0 m in BH5 (Fig. 9a). Boreholes 4 and 5 have relatively deeper cavities at depths of 6.50–7.0 m. The deeper cavity in BH5 (6.5–7.0 m depths), in particular, is found in a low-RQD limestone although cavities form also in relatively higher RQD rocks (Fig. 9). On the other hand, BH1 has no cavities at all. The permeability test confirmed a substantial amount of seepage at BH2, BH3, BH4, and BH5, but not at BH1 which showed no loss for the drilling fluids. The water loss was observed at depths between 1.5 to 8.0 m, indicating the presence of cavities, which represent gaps within the shallow limestone. A rapid drop in the water head was observed at the beginning of the test at BH5 (Fig. 8) followed by a slowly falling head at subsequent time. The estimated permeability coefficient at BH5 is  $1.93 \text{ cm/sec}$ , which is relatively large. Moreover, backfill grout and large water inflows have been met in some excavations supporting the likelihood of interconnected water paths being formed through a comprehensive solution scheme. The TCR values are low and range from 0.0 to 17%. At the top 2 m, RQD values are very low (not exceeding 19%) in boreholes 2–5, indicating poor rock quality (Deere 1964).

According to the drilling information and investigations of RQD and TCR, the subsurface profile is composed mainly of two main layers. The upper layer is composed of crushed, highly weathered limestone, gravel, sand and boulders with an average thickness of 0.7 m. The underlying lower layer

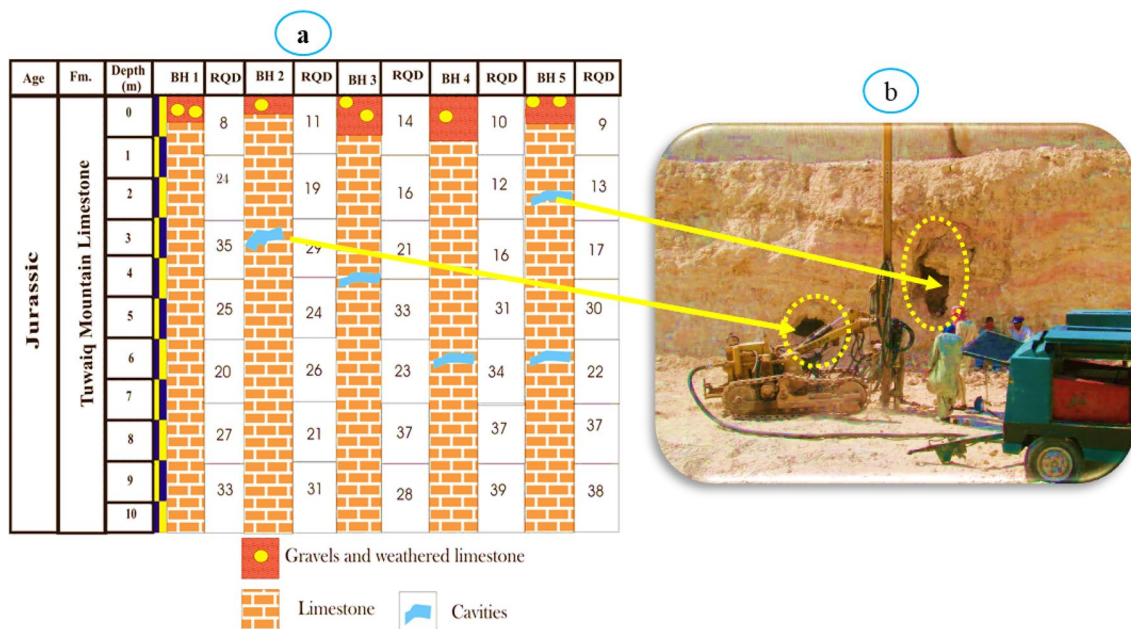


**Fig. 9** Subsurface log of five 10-m-deep boreholes **a** with solution cavities in the Tuwaiq Mountain Limestone, (RQD rock quality designation). **b** A field photo revealing the presence of cavities after trenching

is composed of hard, cavernous, pale yellow, creamy, and fractured limestone bedrock interbedded with rock fragments. Cavities are encountered at various depths in BHs 2, 3, 4, and 5 and are filled with yellowish red-grinded particles (Fig. 9). According to the classification of Deere (1964) for rocks based on their RQD index, the studied site is underlain by very poor to poor limestone bedrocks.

The encountered cavities and fractured limestones are also detected on the GPR images as displaced hyperbolic reflections (Fig. 6b, d, f). The sharp changes from low to high reflectivity result normally from changes in the nature of the material, such as increases or decreases in sand/clay content, changes from carbonate to re-enforced material or even the surface disturbance creating a disturbed radar signal. The detected GPR anomalies cannot result from subsurface infrastructure because their linear coherence is missing. This implies that these features represent only changes in the nature of the limestone rock such as weathering, weak zones, or cavities. The sharp, laterally-extending reflectivity feature (Fig. 6b, d, f) corresponds to the contact between the top native soil and the underlying, more compact layers. On the other hand, the sharp lateral/vertical contrast in amplitude within native rock layers may represent weak/fractured strata, void, and/or cavity. The solution features in the retrieved cores (Fig. 7d) are thus consistent with the GPR anomalies as well as the borehole investigations. Moreover, the detected subsurface cavities are perhaps indications for major ones at deeper levels. Such major cavities can appear clearly by drilling or trenching (Fig. 9b). In this way, the surface GPR investigations confirmed the drilling data at the 5 boreholes. This practice has been applied by many researchers such as Gutiérrez et al. (2011), Pueyo et al. 2009, 2013, 2014; and Pueyo Anchuela et al. (2015).

## Conclusions and recommendations

Both geophysical and borehole investigations have been carried out to detect the near-surface cavities and sinkholes in Ar-Riyadh city, KSA. The drilled boreholes unraveled the subsurface geology of the area. Five cavities at depths of 2.5–7 m were detected underneath the ground at four boreholes. No cavities were detected beneath BH1. Two layers are detected in the 10-m-deep boreholes; the first of which is composed of crushed, highly weathered, limestone, gravel, sand, and boulders (with an average thickness of 0.7 m), while the second layer is composed of hard cavernous, pale yellow to creamy fractured limestone bedrock. This limestone layer contains some rock fragments and some cavities which are filled with yellowish red-grinded particles.

Borehole investigations helped to outline the extent of the underground zones affected by karsts so that possible mitigation actions can be taken in due time. Borehole data

are generally consistent with the GPR results indicating the significant application of the two techniques for cavity detection in karstic areas. Engineering constructions, related excavation works, time constraints, and subsequent costs must rely on detailed geophysical, geological, and borehole investigations before final decisions are taken. The combined use of GPR and borehole testing methods enabled the identification of hidden karstic features down to a depth of 10 m in the investigated area.

Based on the findings of the present study, the following recommendations are proposed:

1. Buildings should be constructed either on reinforced concrete isolated footings, and/or mat foundations, and/or slab, reinforced strip, and ring-beam foundations. The role of these foundations is to distribute the load of a super-structure over large areas.
2. Cement-sand grouting should be implemented down to depths that are three times the maximum footing breadth to ensure the stabilization of the whole rock mass beneath the foundations.
3. Caving probes should be executed before grouting. Also, the ground could be improved by compaction and/or injection of the grout which will increase the strength as well as the bearing capacity of the ground.
4. Tensile geogrids are good remedial measures for linear infrastructures like roads and railways in the sub-base and embankments. These will help in preventing catastrophic collapses.
5. Detailed site investigations are required to detect and assess karst-related hazards such as tilting, cracking, sloping floors, sheared doors, window openings, bulging walls as well as damage by subsidence leading to demolish and to provide cost-effective engineering solutions for each new urban construction.

**Acknowledgements** The authors would like to thank Prof. Alaa Mustafa, Professor of Sedimentary Petrology, Geology Department, Faculty of Science, Al-Azhar University (Assiut Branch), for his critical and constructive comments and suggestions which greatly improved the manuscript. The authors would like to express their gratitude to the Ministry of Education and the Deanship of Scientific Research at Najran University, The Kingdom of Saudi Arabia, for their financial and technical support under code number (NU/SERC/10/559). They are also greatly indebted to the Editor of Carbonates and Evaporites and the anonymous reviewers for their valuable time and the comments they raised that have improved the rigor of the work.

## References

- Abd El Aal AK (2017) Identification and characterization of near surface cavities in Tuwaiq Mountain Limestone, Riyadh, KSA, 'detection and treatment. *Egypt J Petrol* 26:215–223

- Abd El Aal AK, Masoud AA (2017) Impacts of karst phenomena on engineering properties of limestone foundation bed, Ar Riyadh. Saudi Arabia Arab J Geosci 10:347. <https://doi.org/10.1007/s12517-017-3089-7>
- Abd El Aal AK, Nabawy BS, Aqeel A, Abidi A (2020) Geohazards assessment of the karstified limestone cliffs for safe urban constructions, Sohag, West Nile Valley, Egypt. J Afr Earth Sci 161:103671. <https://doi.org/10.1016/j.jafrearsci.2019.103671>
- Abdeltawab S (2013) Karst limestone foundation geotechnical problems, detection and treatment: case studies from Egypt and Saudi Arabia. Int J Sci Eng Res 4:376–387
- Al-Sayari SS, Zötl JG (eds) (1978) Quaternary period in Saudi Arabia. Springer, Wein, p 311
- Amin A, Bankher K (1997) Karst hazard assessment of eastern Saudi Arabia. Nat Hazards 15:21–30
- Annan AP (2001) Ground penetrating radar workshop notes. Sensors and Software, Ontario, p 192
- Annan AP, Cosway SW, Redman JD (1991) Water table detection with ground-penetrating radar (abstract). Meet Soc Explor Geophys 61:494–496
- Annan AP, Davis JL (1992) Design and development of a digital ground penetrating radar system, In: Pilon J (Eds), Ground penetrating radar. Geol Sur Can 15–23: 90–4
- Audru CJ, Bano M, Begg J, Berryman K, Henrys S, Niviere B (2001) GPR investigations on active faults in urban areas: the Georise-NZ project in Wellington, New Zealand. Earth Planet Sci 333:447–454
- BS 5930 (2015) Code of practice for ground investigations. The British Standards Institution, BSI Standards Limited. ISBN 9780580800627
- Cueto M, López-Fernández C, Pando L, Arias D (2019) Engineering geological assessment using geochemical, mineralogical and petrographic analysis along the riyadh metro line 3 (Saudi Arabia), In: Kallel A et al. (Eds) Recent advances in geo-environmental engineering, geomechanics and geotechnics, and geohazards, Springer, Cham. [https://doi.org/10.1007/978-3-030-01665-4\\_36](https://doi.org/10.1007/978-3-030-01665-4_36)
- Daniels DJ (2014) Ground penetrating radar, IEEE Radar, sonar and navigation series, 15, 2nd edn. The Institution of Electrical Engineers, London, p 716
- Daniels DJ (2005) Ground penetrating radar. Encyclopedia of RF and microwave engineering. <https://doi.org/10.1002/0471654507.eme152>
- Daniels DJ (1996) Surface penetrating radar, Institute of Electrical and Electronic Engineers (IEEE), p 300
- Davis JL, Annan AP (1989) Ground-penetrating radar for high resolution mapping of soil and rock stratigraphy. Geophys Prosp 37:531–551
- Deere DU (1964) Technical description of rock cores. Rock Mech Eng Geol 1:16–22
- Edgell HS (1990) Geological framework of Saudi Arabian groundwater resources. J King Abdulaziz Univ Earth Sci 3:267–286
- Eid HT (2007) A technique for estimating permeability of a randomly fractured rock mass. Acta Geotech 2:97–102. <https://doi.org/10.1007/s11440-007-0029-9>
- El-Qady G, Hafez M, Abdalla AM, Ushijima K (2005) Imaging subsurface cavities using geoelectric tomography and ground-penetrating radar. J Cave Karst Stud 67(3):174–181
- Elawadi E, El-Qady G, Salem A, Ushijima K (2001) Detection of cavities using pole-dipole resistivity technique: memoirs of the Faculty of Engineering. Kyushu Univ 61:101–112
- Festa V, Fiore A, Parise M, Siniscalchi A (2012) Sinkhole evolution in the Apulian karst of southern Italy: a case study, with some considerations on sinkhole hazards. J Cave Karst Stud 74(2):137–147
- Fisher SC, Stewart RR, Jol HM (1996) Ground penetrating radar (GPR) data enhancement using seismic techniques. J Environ Eng Geophys 1:89–96
- Forte E, Pipan M, Casabianca D, Cuia RD, Riva A (2012) Imaging and characterization of a carbonate hydrocarbon reservoir analogue using GPR attributes. J Appl Geophys 81:76–87
- Geophysical Survey Systems Inc (2005) RADAN 6.5 user's manual, Geophysical Sensors and Systems Inc, New Hampshire, USA
- Geophysical Survey Systems Inc (2008) Radan post processing software version 6.5 User's Manual, 12 Industrial Way, Salem, NH 03079
- Gross R, Green A, Holliger K, Horstmeyer H, Baldwin J (2002) Shallow geometry and displacement on the San Andreas Fault near Point Arena based on trenching and 3-D georadar surveying. Geophys Res Lett 29(20):34-1-34–4
- Gutiérrez F, Galve JP, Lucha P, Castañeda C, Bonachea J, Guerrero J (2011) Integrating geomorphological mapping, trenching, InSAR and GPR for the identification and characterization of sinkholes: a review and application in the mantled evaporite karst of the Ebro Valley. Geomorphology 134:144–156
- Hughes GW, Lindsay RF (2017) Micropalaeontology and sedimentology of an inter-evaporite Arab-C carbonate exposure, Riyadh, Saudi Arabia. Carbonates Evaporites. <https://doi.org/10.1007/s13146-017-0345-6>
- Hughes GW, Naji N (2008) Sedimentological and micropaleontological evidence to elucidate post-evaporitic carbonate paleoenvironments of the Saudi Arabian latest Jurassic. Volumina Jurassica 6:61–73
- Knight RJ, Nur A (1987) The dielectric constant of sandstones 60 kHz to 4 MHz. Geophysics 52:644–654
- Mochales T, Casas AM, Pueyo EL, Pueyo Ó, Román MT, Pocoví A, Soriano MA, Ansón D (2008) Detection of underground cavities by combining gravity, magnetic and ground penetrating radar surveys: a case study from the Zaragoza area NE Spain. Environ Geol 53(5):1067–1077
- Neal A (2004) Ground penetrating radar and its use in sedimentology: principles, problems and progress. Earth Sci Rev 66:261–330
- Nicholls K (2012) Discussion on 'measurement of total core recovery; dealing with core loss and gain.' Q J Eng Geol Hydrogeol 45(3):391
- Olhoef GR (1994) Modeling out-of-plane scattering effects: Proceedings of the 5th International Conference on Ground Penetrating Radar, 133–144. <https://doi.org/10.3997/2214-4609-pdb.300.11>
- Oppenheim AV, Willsky AS, Nawab SH (2003) Signals and systems, Pearson Education.
- Powers RW, Ramirez LF, Redmond CD, Elberg JFL (1966) Geology of the Arabian Peninsula: sedimentary geology of Saudi Arabia. S Geol Surv Prof Pap 560-D
- Pueyo Anchuela Ó, Casas-Sainz AM, Pocoví-Juan A, Garbí HG, Calvín P (2014) Characterization of the karstic process in an urban environment using GPR surveys. J Mater Civil Eng. [https://doi.org/10.1061/\(ASCE\)MT.1943-5533.0001072](https://doi.org/10.1061/(ASCE)MT.1943-5533.0001072)
- Pueyo Anchuela Ó, Julián PL, Casas-Sainz AM, Liesa CL, Pocoví-Juan A, Cordero JR, Benedicto JAP (2015) Three-dimensional characterization of complex mantled karst structures: decision making and engineering solutions applied to a road overlying evaporate rocks in the Ebro Basin (Spain). Eng Geol 193:158–172. <https://doi.org/10.1016/j.enggeo.2015.04.022>
- Pueyo Anchuela Ó, Pocoví Juan A, Casas-Sainz AM, Ansón-López D, Gil-Garbí H (2013) Actual extension of sinkholes: considerations about geophysical, geomorphological and field inspection techniques in urban planning projects in the Ebro basin (NE Spain). Geomorphology 189:135–149
- Pueyo Anchuela Ó, Pocoví Juan A, Soriano MA, Casas-Sainz AM (2009) Characterization of karst hazards from the perspective of the doline triangle using GPR—examples from Central Ebro Basin (Spain). Eng Geol 108:225–236
- Sharief FA, Khan MS, Magara K (1991) Outcrop–subcrop sequence and diagenesis of Upper Jurassic Arab Hith formations, central Saudi Arabia. J King Abdulaziz Univ 4:105–136

- Smith D (1986) Application of the pole-dipole resistivity technique in the detection of solution cavities beneath highways. *Geophys* 51:833–837
- Takahashi K (2006) Detection and localization of subsurface objects by ground penetrating radar. PhD thesis, Tohoku Univ, Japan
- Trivedi A (2015) Computing in situ strength of rock masses based upon RQD and modified joint factor: using pressure and damage sensitive constitutive relationship. *J Rock Mech Geotech Eng* 7(5):540–565
- Valentine S, Norbury D (2011) Measurement of total core recovery; dealing with core loss and gain. *Q J Eng Geol Hydrogeol* 44:397–403. <https://doi.org/10.1144/1470-9236/10-009>
- Vaslet D, Al-Muallem MS, Maddah SS, Brosse JM, Fourniguet J, Breton JP, Le Nindre YM (1991) Geologic map of the Ar Riyadh quadrangle, sheet 24 I, Kingdom of Saudi Arabia. Saudi Arabian Deputy Ministry for Mineral Resources Geoscience Map GM-121, pp 54, scale 1:250,000
- Youssef AM, Al-Harbi HM, Gutiérrez F, Zabramwi YA, Bulkhi AB, Zahrani SA, Bahamil AM, Zahrani A, Otaibi J, El Haddad BA (2016) Natural and human-induced sinkhole hazards in Saudi Arabia: distribution, investigation, causes and impacts. *Hydrogeol J.* <https://doi.org/10.1007/s10040-015-1336-0>
- Youssef AM, El-Kaliouby H, Zabramawi YA (2012) Integration of remote sensing and electrical resistivity methods in sinkhole investigation in Saudi Arabia. *J Appl Geophys* 87:28–39
- Youssef AM, Pradhan B, Sabtan AA, El-Harbi HM (2011) Coupling of remote sensing data aided with field investigations for geological hazards assessment in Jazan area, Kingdom of Saudi Arabia. *Environ Earth Sci* 65(1):119–130

**Publisher's Note** Springer Nature remains neutral with regard to jurisdictional claims in published maps and institutional affiliations.